Optical fingerprints of two-dimensional interlayer-sliding multiferroic materials

Hong-Miao Zhao,[1] Hang Zhou,[1,2] Wei Gan ,[1] Hui Han,[1,3] Hui Li,[1,3] and Rui-Chun Xiao [1,3,*]

[1]*Institute of Physical Science and Information Technology, Anhui University, Hefei 230601, China*

[2]*Key Laboratory of Materials Physics, Institute of Solid State Physics, Hefei Institutes of Physical Science, Chinese Academy of Sciences, Hefei 230031, China*

[3]*Anhui Provincial Key Laboratory of Magnetic Functional Materials and Devices, School of Materials Science and Engineering, Anhui University, Hefei 230601, China*

Recently, two-dimensional (2D) interlayer-sliding multiferroic materials, consisting of two nonferroelectric monolayer ferromagnetic (FM) layers with specific interlayer stacking and sliding, have garnered significant interest for their potential in expanding the range of 2D multiferroics. However, the low-dimensional nature of 2D multiferroic materials results in relatively weak magnetic and ferroelectric (FE) properties, posing challenges for traditional detection methods in characterizing these two order parameters. In this work, we study the optical fingerprints of 2D interlayer-sliding multiferroic materials. By utilizing an abstract bilayer model, we demonstrate that the four multiferroic states ($P_\uparrow N_\uparrow$, $P_\uparrow N_\downarrow$, $P_\downarrow N_\downarrow$, and $P_\downarrow N_\uparrow$) are interconnected via the horizontal mirror symmetry $\hat{M}_z$, time-reversal symmetry $\hat{T}$, and their combination symmetries $\hat{M}_z\hat{T}$. Subsequently, we analyze the tensor elements associated with the optical Kerr effect and second harmonic generation (SHG) effect in multiferroic states, revealing a strong correlation between both the Kerr effect and SHG effect and the multiferroic orders of 2D interlayer-sliding multiferroic materials, as well as the presence of distinct optical characteristics across different multiferroic states. Using VSe$_2$ and MnBi$_2$Te$_4$ as two representative 2D interlayer-sliding multiferroic materials, we further validate the intricate correlations between the symmetries and optical properties. Our research provides theoretical guidance for characterizing 2D interlayer-sliding multiferroic materials by means of optical methods.

I. INTRODUCTION

Spontaneous spin polarization ferromagnetic (FM) order and spontaneous electric polarization ferroelectric (FE) order are two main order parameters in condensed matter physics. Multiferroic materials, as a special kind of quantum material with these two order parameters, possess profound physical significance as well as promising application prospects in the fields of electronics and spintronics. From the perspective of symmetry breaking, multiferroic materials with ferroelectricity and magnetism need to break both inversion symmetry $\hat{P}$ and time-reversal symmetry $\hat{T}$ simultaneously. In addition, the existence of the d^0 rule [1] leads to the mutual exclusion of the coexistence of magnetism and ferroelectricity. At the same time, the existence of depolarization field, surface energy effect, and electron screening leads to the scarcity of intrinsic two-dimensional (2D) multiferroic materials [2,3].

The concept of interlayer-sliding ferroelectricity [4–11] provides an alternative method for the construction of 2D multiferroic materials and expands the family of 2D multiferroics. Recently, lots of 2D interlayer-sliding multiferroic materials (e.g., VS$_2$ [12], VSe$_2$ [13], FeCl$_2$ [13], MnBi$_2$Te$_4$ [14–17], MnSe [18], Cr$_2$Ge$_2$Te$_6$ [19], Fe$_3$GeTe$_2$ [19], and CrI$_3$ [13,20]) have been predicted. The mechanism of the ferroelectricity in 2D interlayer-sliding multiferroic materials differs from those in conventional ones. The ferroelectricity arises from the interlayer sliding of two nonferroelectric monolayer ferromagnetic materials [12–20]. The ferroelectric polarization results in a Coulomb-potential difference for the magnetic atoms in the top and bottom layers, leading to a weak uncompensated magnetic moment under the antiferromagnetic (AFM) configuration.

Although lots of 2D interlayer-sliding multiferroic materials have been predicted theoretically, the weak magnetic and FE orders make them difficult to be detected by the traditional magnetic and ferroelectric measurement methods, which hinders the progress in experiments. The Kerr effect and second harmonic generation (SHG) effect, within the realm of optics, exhibit remarkable sensitivity to the violation of $\hat{T}$ symmetry and $\hat{P}$ symmetry in condensed matter physics. Therefore, they show strong characterization capabilities for magnetism [21–24] and ferroelectricity [25,26]. Consequently, the Kerr effect and SHG effect show the possibility to detect the order parameters for the 2D interlayer-sliding multiferroic materials.

In this work, we investigated the optical properties (Kerr effect and SHG effect) of 2D interlayer-sliding multiferroic materials using symmetry analysis (including abstract bilayer model [10] and isomorphic group method [27]) and first-principles calculations. We found that the Kerr effect and SHG effect are tightly dependent on the multiferroic order in

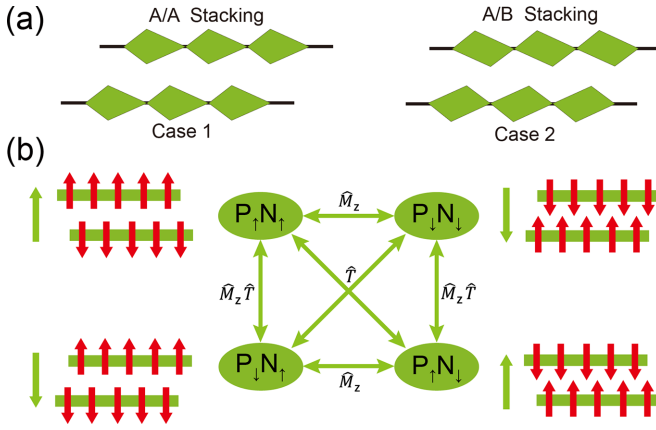*Contact author: xiaoruichun@ahu.edu.cn

FIG. 1. (a) The interlayer-stacking and -sliding methods to achieve the interlayer-sliding multiferroicity. In the case of monolayers lacking $\hat{P}$ symmetry but possessing $\hat{M}_z$ symmetry (case 1), the A/A stacking mode is utilized. On the other hand, for monolayers with $\hat{P}$ symmetry but lacking $\hat{M}_z$ symmetry (case 2), the A/B stacking mode is employed. (b) The four multiferroic states ($P_\uparrow N_\uparrow$, $P_\uparrow N_\downarrow$, $P_\downarrow N_\downarrow$, and $P_\downarrow N_\uparrow$) and the interconnected symmetry. The red arrows represent the direction of magnetic moments, and the green arrows stand for the direction of out-of-plane FE polarization.

2D interlayer-sliding multiferroic materials. This dependence leads to unique optical fingerprints of different multiferroic states. These optical properties are beneficial for the detection of 2D interlayer-sliding multiferroic materials in experiments, and the design of optoelectronic devices based on them.

II. SYMMETRY ANALYSIS

Next, we will discuss the process of achieving interlayer-sliding multiferroicity by employing interlayer-stacking and -sliding techniques with 2D nonferroelectric monolayer FM materials. Currently, most of the monolayer FM materials that have been discovered are nonpolar and nonferroelectric. The crystal structures of these materials mainly fall into two cases. Case 1 is monolayers without $\hat{P}$ symmetry but with horizontal mirror symmetry $\hat{M}_z$, e.g., VS$_2$ [12], VSe$_2$ [13], and Fe$_3$GeTe$_2$ [19,28]. Case 2 is monolayers with $\hat{P}$ symmetry but without $\hat{M}_z$ symmetry, e.g., FeCl$_2$ [13], MnBi$_2$Te$_4$ [14–17], CrI$_3$ [13,20,29], Cr$_2$Ge$_2$Te$_6$ [19,30], and MnSe [18]. Using the bilayer abstract model [10] that we proposed earlier, the interlayer multiferroicity can be attained by employing interlayer-stacking and -sliding techniques. Specifically, for case 1, the A/A stacking mode is employed, while for case 2, the A/B stacking mode (where $B = \hat{C}_{2z}A$; A and B represent crystal types) is utilized to achieve interlayer-sliding multiferroicity, as illustrated in Fig. 1(a). Furthermore, the positive and negative FE states are connected by the $\hat{M}_z$ symmetry [10], that is

$$P_\uparrow = \hat{M}_z P_\downarrow, \tag{1}$$

where $P_\uparrow$ ($P_\downarrow$) represents the direction of FE polarization towards the positive (negative) z-axis direction.

In the case of stacking monolayer FM materials into a bilayer configuration, it commonly results in an AFM arrangement between the interlayers [12–20]. As a result,

the combination of FE and AFM states gives rise to four distinct multiferroic states, namely $P_\uparrow N_\uparrow$, $P_\uparrow N_\downarrow$, $P_\downarrow N_\downarrow$, and $P_\downarrow N_\uparrow$. Here, N represents the Néel vector, which represents the difference in magnetic moments between the top and bottom layers, i.e., $N = M_{\text{top}} - M_{\text{bottom}}$. $N_\uparrow$ denotes the Néel vector towards the positive z-axis direction (i.e., the magnetic moment of the upper layer is positive and the magnetic moment of the lower layer is negative along the z axis). Conversely, $N_\downarrow$ represents the Néel vector directing towards the negative z-axis direction.

According to Eq. (1), the positive and negative FE polarization are connected by the $\hat{M}_z$ symmetry. Meanwhile, the transformation of the Néel vector under $\hat{M}_z$ symmetry is given by

$$\hat{M}_z N = \hat{M}_z(M_{\text{top}} - M_{\text{bottom}}) = M_{\text{bottom}} - M_{\text{top}}. \tag{2}$$

The equality holds because the $\hat{M}_z$ symmetry operation switches the order of the two layers but does not change the z component of the magnetic moment. Therefore, under $\hat{M}_z$ symmetry operations, the Néel vector also reverses its direction, i.e.,

$$\hat{M}_z N_\downarrow = N_\uparrow. \tag{3}$$

Additionally, FE polarization remains unchanged under $\hat{T}$ symmetry ($\hat{T}P_\uparrow = P_\uparrow$), whereas the Néel vector reverses direction under $\hat{T}$ symmetry ($\hat{T}N_\uparrow = N_\downarrow$). Based on these symmetry considerations, we obtain that

$$\hat{M}_z P_\uparrow N_\uparrow = P_\downarrow N_\downarrow, \tag{4}$$

$$\hat{T} P_\uparrow N_\uparrow = P_\uparrow N_\downarrow, \tag{5}$$

$$\hat{M}_z \hat{T} P_\uparrow N_\uparrow = P_\downarrow N_\uparrow. \tag{6}$$

Therefore the four multiferroic states are interconnected through the $\hat{M}_z$ symmetry, $\hat{T}$ symmetry, and the $\hat{M}_z\hat{T}$ symmetry, as demonstrated in Fig. 1(b).

Interlayer sliding results in out-of-plane FE polarization, which can give rise to a weak but uncompensated magnetic moment in the AFM configuration. Consequently, the 2D interlayer-sliding multiferroic materials also exhibit the Kerr effect, which is similar to the anomalous Hall effect [15–17] observed in the experiments. The anomalous photoconductivity associated with this Kerr effect corresponds to the σ_{xy}^A component, if the light irradiates perpendicularly to the material. The anomalous photoconductivity σ_{xy}^A remains invariant under the $\hat{M}_z$ symmetry. Nevertheless, it reverses its sign under $\hat{T}$ or $\hat{M}_z\hat{T}$ symmetry, due to its odd nature under $\hat{T}$ symmetry operation, as shown in Table I. Since the multiferroic order can be manipulated by the electric or magnetic fields, the Kerr signal switches accordingly. Given this unique characteristic, the 2D interlayer-sliding multiferroic materials hold applications in optical storage devices. In contrast to traditional magneto-optical memories, which rely on magnetic-writing-optical-reading [31–33], the interlayer-sliding multiferroic material memory offers a more convenient approach, enabling electrical-writing-optical-reading [34].

In 2D interlayer-sliding multiferroic materials, the breaking of $\hat{P}$ symmetry gives rise to the emergence of the SHG effect in this system. Next, we will analyze the characteristics of the SHG effect. The $\hat{M}_z$ symmetry operator

TABLE I. The relationship of SHG and Kerr coefficients within different multiferroic states. We assign the even and odd components of the SHG and σ_{xy}^A in the $P_\uparrow N_\uparrow$ state with "+" sign, and +/− in the other multiferroic states indicates the coefficient invariant/reverse its sign.

Symmetry relation with $P_\uparrow N_\uparrow$	In-plane SHG $[\chi_{ijk}^{(2)}, i, j, k \in (x, y)]$		Out-of-plane SHG ($\chi_{zzz}^{(2)}$), in- and out-of-plane SHG $[\chi_{ijk}^{(2)}, i, j, k \in (x, y, z)]$		Kerr σ_{xy}^A
	even	odd	even	odd	
$P_\uparrow N_\uparrow$ $\quad$ $\hat{E}$	+	+	+	+	+
$P_\uparrow N_\downarrow$ $\quad$ $\hat{T}$	+	−	+	−	−
$P_\downarrow N_\uparrow$ $\quad$ $\hat{M}_z\hat{T}$	+	−	−	+	−
$P_\downarrow N_\downarrow$ $\quad$ $\hat{M}_z$	+	+	−	−	+

leads to the in-plane SHG tensor elements $[\chi_{ijk}^{(2)}, i, j, k \in (x, y)]$ remaining unchanged, while it reverses the out-of-plane SHG tensor elements ($\chi_{zzz}^{(2)}$) and the mixed in- and out-of-plane SHG tensor elements $[\chi_{ijk}^{(2)}, i, j, k \in (x, y, z)$, where there is one and only one z component present]. Additionally, the $\hat{T}$ symmetry is broken; the SHG tensor elements therefore should be categorized into $\hat{T}$-even (i type, χ_{ijk}^{even}) and $\hat{T}$-odd (c type, χ_{ijk}^{odd}) components [35]. The even components remain unchanged under $\hat{T}$ symmetry, while the odd components reverse their signs under $\hat{T}$ symmetry. Based on the above rules, we can establish the relationship between SHG coefficients of the four multiferroic states, as summarized in Table I. The different SHG behaviors in diverse magnetic orders can be used to distinguish the multiferroic domain, as studied in the following.

III. CALCULATION METHODS

Next, we will use two 2D interlayer-sliding multiferroic materials, VSe$_2$ of case 1 and MnBi$_2$Te$_4$ of case 2, as examples to verify our symmetry analysis. The first-principles calculations based on density functional theory (DFT) are performed by using the Vienna *ab-initio* Software Package (VASP) [36,37]. General gradient approximation (GGA) according to the Perdew-Burke-Ernzerhof (PBE) functional is used. Spin-orbit coupling (SOC) effects are considered for all the materials. $U_{\text{eff}} = 1.2$ eV (4.0 eV) is set for V (Mn) atoms in the VSe$_2$ (MnBi$_2$Te$_4$) calculations. The DFT Bloch wave functions are iteratively transformed into maximally localized Wannier functions by the WANNIER90 package [38,39]. The optics coefficients are calculated by our own program WRFP (WANNIER90 Response Function Package), based on the effective tight-binding Hamiltonian obtained by WANNIER90. The methodology of SHG and Kerr effects are introduced in Sec. V of the Supplemental Material [40] (see also Refs. [41–45] therein). The symmetries of magnetic materials were analyzed with the help of the FINDSYM [46] and Bilbao Crystallographic Server [47] website.

IV. FIRST-PRINCIPLES CALCULATION RESULTS

A. Bilayer VSe$_2$

The monolayer VSe$_2$ crystal structure exhibits $\hat{M}_z$ symmetry and $\hat{C}_3$ rotational symmetry, but no $\hat{P}$ symmetry, and hence it does not possess FE polarization. However, when two identical layers of VSe$_2$ are stacked and slid in the

manner depicted in Fig. 1(a), their $\hat{M}_z$ symmetry is broken, leading to out-of-plane FE polarization [10,12,13]. The FE states can be switched by interlayer sliding along the armchair direction.

The magnetic space group of the bilayer VSe$_2$ belongs to $P3m'1$; as a result, the anomalous photoconductivity σ_{xy}^A of the bilayer VSe$_2$ is nonzero (see Sec. IV of the Supplemental Material for details [40]; see also Refs. [27,48] therein). The anomalous photoconductivity σ_{xy}^A of the four multiferroic states of the bilayer VSe$_2$ are shown in Fig. 2(a). We find that anomalous photoconductivity σ_{xy}^A keeps invariant or switches among the different multiferroic states, whose behaviors are consistent with the results in Table I. The anomalous photoconductivity σ_{xy}^A can be observed by Kerr effects in experiments, and the Kerr effect can be tuned by either electric or magnetic fields. The anomalous photoconductivity σ_{xy}^A and anomalous Hall conductivity share similar symmetry requirements. Therefore, one can expect that this bilayer VSe$_2$ should also exhibit the anomalous Hall effect under suitable electric doping, whose mechanism is similar to the Hall effects observed in the bilayer AFM MnBi$_2$Te$_4$ [15–17,49,50].

We investigate the symmetry-constrained SHG tensor of bilayer VSe$_2$ with the isomorphic group method [27]. The magnetic point group $3m'$ of VSe$_2$ imposes restrictions on the even (χ_{ijk}^{even}) and odd (χ_{ijk}^{odd}) components of SHG, and these two restrictions on χ_{ijk}^{even} and χ_{ijk}^{odd} are equivalent to the nonmagnetic point groups $3m$ and 32, respectively (see Sec. III of the Supplemental Material for details [40], and see also Refs. [27,35] therein). This implies that the nonzero even components of SHG tensor are χ_{zzz}^{even}, $\chi_{xxz}^{\text{even}}(= \chi_{xzx}^{\text{even}} = \chi_{yyz}^{\text{even}} = \chi_{yzy}^{\text{even}})$, $\chi_{zxx}^{\text{even}}(= \chi_{zyy}^{\text{even}})$, and $\chi_{yyy}^{\text{even}}(= -\chi_{xxy}^{\text{even}} = -\chi_{xyx}^{\text{even}} = -\chi_{yxx}^{\text{even}})$, while the nonzero odd components stratify the $\chi_{xxx}^{\text{odd}} = -\chi_{xyy}^{\text{odd}} = -\chi_{yxy}^{\text{odd}} = -\chi_{yyx}^{\text{odd}}$ and $\chi_{xyz}^{\text{odd}} = \chi_{xzy}^{\text{odd}} = -\chi_{yxz}^{\text{odd}} = -\chi_{yzx}^{\text{odd}}$. The calculated results are shown in Fig. 2(b) and are also consistent with our symmetry analysis results.

Compared to the monolayer VSe$_2$, we observe that the SHG coefficients of even components (χ_{xxy}^{even}, χ_{yxx}^{even}, and χ_{yyy}^{even}) are approximately twice as large as the bilayer, while the SHG coefficients of odd components (χ_{xxx}^{odd}, χ_{xyy}^{odd}, and χ_{yxy}^{odd}) are significantly smaller than those of monolayer. Furthermore, the $\hat{T}$-odd SHG coefficients of the bilayer are much smaller than the even in-plane SHG coefficients. The computational results for the monolayer are presented in Supplemental Material [40] Fig. S6 (see also Ref. [27] therein).
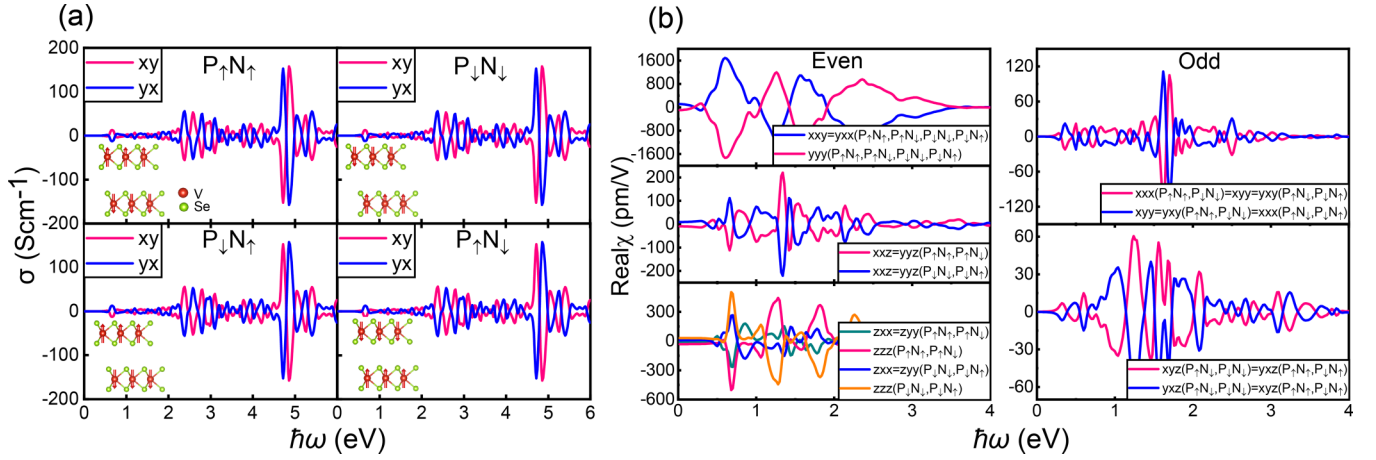
FIG. 2. Calculated (a) anomalous photoconductivity σ_{xy}^A and (b) SHG coefficients of the bilayer VSe$_2$ in four multiferroic states. The calculated SHG and Kerr coefficients within different multiferroic states are consistent with the results in Table I.

Besides, recently theoretical works predicted that 2D materials like bilayer VS$_2$ [12] and Fe$_3$GeTe$_2$ [19,28] possess similar interlayer-sliding ferroelectricity akin to case 1, as well as sharing the same symmetry. Consequently, it is anticipated that these materials will also exhibit similar Kerr and SHG effects.

MnSe [18] possess interlayer-sliding ferroelectricity, which falls into case 2. Consequently, it is anticipated that these materials are also expected to exhibit Kerr effects and SHG effects similar to those of MnBi$_2$Te$_4$.

### B. Bilayer MnBi$_2$Te$_4$

The monolayer MnBi$_2$Te$_4$ crystal structure exhibits $\hat{P}$ symmetry, but lacks $\hat{M}_z$ symmetry. However, by stacking identical layers of MnBi$_2$Te$_4$, rotated by 180° relative to each other in the xy plane, and subsequently sliding them, the $\hat{P}$ symmetry is broken, resulting in out-of-plane FE polarization [14–17], as shown in Fig. 3(a). Therefore, bilayer MnBi$_2$Te$_4$ belongs to case 2 in Fig. 1(a). The magnetic point groups of bilayers MnBi$_2$Te$_4$ and VSe$_2$ are the same, i.e., $3m\prime$, leading to the same symmetry-constrained SHG tensor and anomalous photoconductivity σ_{xy}^A in both materials despite the fact that the magnetic point groups of their respective monolayers are different. There exists extensive prior research on the basic physical properties of interlayer-sliding MnBi$_2$Te$_4$, such as ferroelectricity, magnetism, electric structure, and layer-polarized anomalous Hall effect [14–17]. We also conducted a detailed analysis of the ferroelectric polarization and magnetic properties in the Supplemental Material [40] (see Fig. S2 and Table SI), consistent with previous works [12,17].

As shown in Fig. 3(b), our calculations for bilayer MnBi$_2$Te$_4$ reveal that when only one order parameter (FE or Néel) changes, the anomalous photoconductivity σ_{xy}^A reverses its sign. However, when FE and Néel order parameters undergo a sign reversal, the anomalous photoconductivity σ_{xy}^A remains invariant. These results align with our symmetry analysis (see Table I). Meanwhile, the calculated SHG coefficients are shown in Fig. 3(c). Nevertheless, we find that the SHG coefficients of bilayer MnBi$_2$Te$_4$ in the low frequency are particularly significant, suggesting a potential link to its topological properties [51,52].

Similarly, theoretical predictions suggest that bilayer materials such as FeCl$_2$ [13], CrI$_3$ [13,20], Cr$_2$Ge$_2$Te$_6$ [19,30], and
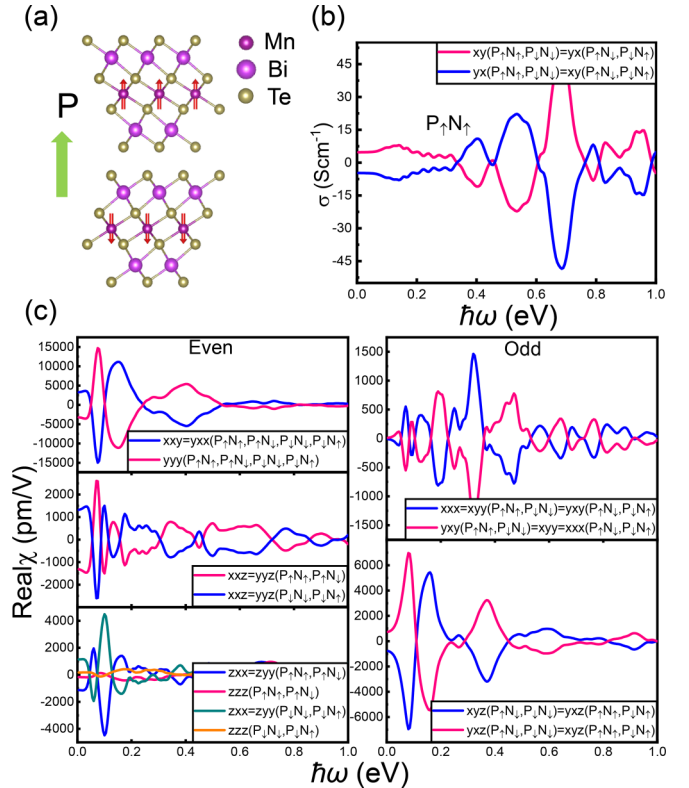
FIG. 3. (a) Crystal structure of the multiferroic state $P_\uparrow N_\uparrow$ of MnBi$_2$Te$_4$. The red arrows represent the direction of magnetic moments and the green arrow represent the direction of out-of-plane FE polarization. (b) Anomalous photoconductivity σ_{xy}^A of the multiferroic states. (c) SHG coefficients of the even and odd parts of the four multiferroic states. We have symmetrized the in-plane SHG tensor elements of the odd components ($P_\uparrow N_\uparrow + P_\downarrow N_\downarrow - P_\downarrow N_\uparrow - P_\uparrow N_\downarrow /4$).

V. DISCUSSION AND CONCLUSIONS

As demonstrated above, each multiferroic state possesses a unique anomalous photoconductivity σ_{xy}^A and SHG characteristics, which give rise to distinctive optical fingerprints for 2D interlayer-sliding multiferroic materials. Specifically, the switch of anomalous photoconductivity σ_{xy}^A causes the reversal of the Kerr signal in experiments. However, the presence of numerous nonzero SHG tensor elements and their complexity greatly surpass those of anomalous photoconductivity σ_{xy}^A, resulting in richer SHG behaviors than those of the Kerr effect.

To comprehensively capture the multiferroic states by means of the SHG effect, all SHG tensor elements should participate and interfere. Therefore, we should employ the oblique incident SHG method in experiments to detect the order parameter of 2D interlayer-sliding multiferroic materials, as shown in Fig. 4(a). Our analysis revealed that the *PPP* and *PSS* configuration can satisfy the requirement (see Sec. VII of the Supplemental Material for details [40]). The *PPP* polarization-resolved SHG patterns of four multiferroic states are shown in Fig. 4(b). Notably, the SHG patterns resemble flowers with six petals. The petals are nonuniform, because of the interference of the in-plane, mixed in- and out-of-plane, and out-of-plane SHG coefficients. The SHG flowers exhibits $\hat{C}_3$ rotation symmetry, but are not symmetric about the x axis or the y axis. The misalignment angles relative to the x axis or the y axis are intimately linked to the even and odd SHG coefficients (see Sec. VII of the Supplemental Material for details [40]). Given the fact that the polarization-resolved SHG patterns of each multiferroic state of 2D interlayer-sliding multiferroic materials are different, as shown in Fig. 4(b), we can detect these multiferroic states by means of the oblique incident SHG method in Fig. 4(a). If the positive and negative ferroelectric states in multiferroic materials are interconnected through the inversion symmetry, as the conventional multiferroic materials, the oblique incident SHG technique is unable to distinguish these multiferroic states (see Sec. VIII of the Supplemental Material for details [40]; see also Refs. [53–59] therein). Therefore, the behavior of SHG in the interlayer-sliding multiferroic shows abundant characteristics compared to conventional multiferroic materials.

In summary, with the symmetry analysis of the abstracted bilayer model, we found that the ferromagnetic material of the 2D nonferroelectric monolayer can form four multiferroic states ($P_\uparrow N_\uparrow$, $P_\uparrow N_\downarrow$, $P_\downarrow N_\downarrow$, and $P_\downarrow N_\uparrow$) through interlayer stacking and sliding, and these multiferroic states are interconnected via $\hat{M}_z$, $\hat{T}$, and $\hat{M}_z\hat{T}$ symmetries. Due to the interlayer stacking and sliding breaking the $\hat{P}$ symmetry, 2D interlayer-sliding multiferroic materials produce out-of-plane FE polarization, which leads to weak uncompensated magnetic moments. Consequently, the 2D interlayer-sliding multiferroic materials exhibit the Kerr effect and the SHG effect. Notably, within two representative examples bilayer VSe$_2$ and MnBi$_2$Te$_4$, we demonstrate that each multiferroic state exhibits unique optical signatures. Therefore, our research provides a theoretical guidance for using optical methods to detect 2D interlayer-sliding multiferroic materials.
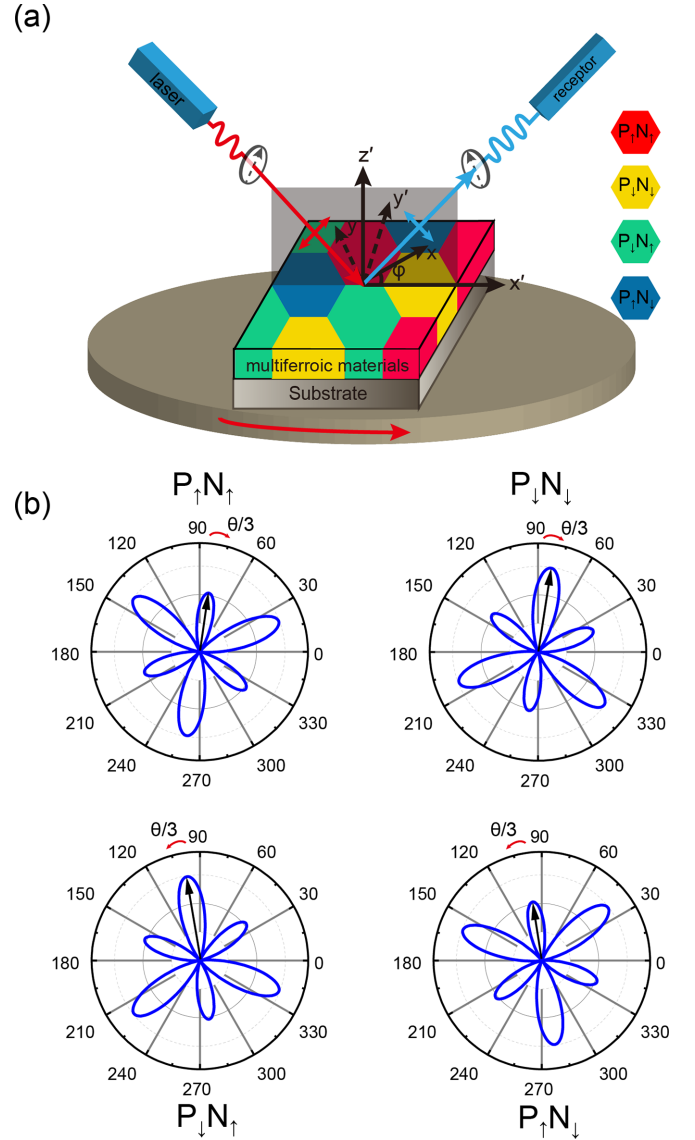

FIG. 4. (a) Illustration of the detection multiferroic states via oblique incident SHG method. The polarization of the fundamental and SHG beams is represented by double arrows lines (*P* polarization), where φ represents the azimuth angle between the x axis and the $x'z'$ plane, where x', y', z' are the laboratory coordinates axis, which keep invariant. (b) Corresponding polarization-resolved SHG pattern with the multiferroic states with *PPP* setting. $E_{PPP}(2\omega) \propto \chi_{xxx}^{\mathrm{odd}} \cos(3\varphi) + \chi_{yyy}^{\mathrm{even}} \sin(3\varphi) + 2\chi_{xxz}^{\mathrm{even}} + \chi_{zxx}^{\mathrm{even}} + \chi_{zzz}^{\mathrm{even}}$, where we set $\chi_{yyy}^{\mathrm{even}} : \chi_{xxx}^{\mathrm{odd}} : (2\chi_{xxz}^{\mathrm{even}} + \chi_{zxx}^{\mathrm{even}} + \chi_{zzz}^{\mathrm{even}}) = 1 : 0.5 : 0.2$. Detailed information is shown in Sec. VII of Supplemental Material [40].

[1] N. A. Hill, Why are there so few magnetic ferroelectrics? J. Phys. Chem. B **104**, 6694 (2000).

[2] C. Tang and A. Du, Perspective on computational design of two-dimensional materials with robust multiferroic coupling, Appl. Phys. Lett. **122**, 130502 (2023).

[3] Y. Gao, M. Gao, and Y. Lu, Two-dimensional multiferroics, Nanoscale **13**, 19324 (2021).

[4] L. Li and M. Wu, Binary compound bilayer and multilayer with vertical polarizations: Two-dimensional ferroelectrics, multiferroics, and nanogenerators, ACS Nano **11**, 6382 (2017).

[5] M. Wu and J. Li, Sliding ferroelectricity in 2D van der Waals materials: Related physics and future opportunities, Proc. Natl. Acad. Sci. USA **118**, e2115703118 (2021).

[6] K. Yasuda, X. Wang, K. Watanabe, T. Taniguchi, and P. Jarillo-Herrero, Stacking-engineered ferroelectricity in bilayer boron nitride, Science **372**, 1458 (2021).

[7] X. Wang, K. Yasuda, Y. Zhang, S. Liu, K. Watanabe, T. Taniguchi, J. Hone, L. Fu, and P. Jarillo-Herrero, Interfacial ferroelectricity in rhombohedral-stacked bilayer transition metal dichalcogenides, Nat. Nanotechnol. **17**, 367 (2022).

[8] M. Vizner Stern, Y. Waschitz, W. Cao, I. Nevo, K. Watanabe, T. Taniguchi, E. Sela, M. Urbakh, O. Hod, and M. Ben Shalom, Interfacial ferroelectricity by van der Waals sliding, Science **372**, 1462 (2021).

[9] A. Weston, E. G. Castanon, V. Enaldiev, F. Ferreira, S. Bhattacharjee, S. Xu, H. Corte-León, Z. Wu, N. Clark, A. Summerfield, T. Hashimoto, Y. Gao, W. Wang, M. Hamer, H. Read, L. Fumagalli, A. V. Kretinin, S. J. Haigh, O. Kazakova, A. K. Geim *et al.*, Interfacial ferroelectricity in marginally twisted 2D semiconductors, Nat. Nanotechnol. **17**, 390 (2022).

[10] R.-C. Xiao, Y. Gao, H. Jiang, W. Gan, C. Zhang, and H. Li, Non-synchronous bulk photovoltaic effect in two-dimensional interlayer-sliding ferroelectrics, npj Comput. Mater. **8**, 138 (2022).

[11] J. Ji, G. Yu, C. Xu, and H. J. Xiang, General theory for bilayer stacking ferroelectricity, Phys. Rev. Lett. **130**, 146801 (2023).

[12] X. Liu, A. P. Pyatakov, and W. Ren, Magnetoelectric coupling in multiferroic bilayer VS$_2$, Phys. Rev. Lett. **125**, 247601 (2020).

[13] C. Zhang, P. Guo, and J. Zhou, Tailoring bulk photovoltaic effects in magnetic sliding ferroelectric materials, Nano Lett. **22**, 9297 (2022).

[14] Y. Ren, S. Ke, W.-K. Lou, and K. Chang, Quantum phase transitions driven by sliding in bilayer MnBi$_2$Te$_4$, Phys. Rev. B **106**, 235302 (2022).

[15] T. Cao, D.-F. Shao, K. Huang, G. Gurung, and E. Y. Tsymbal, Switchable anomalous Hall effects in polar-stacked 2D antiferromagnet MnBi$_2$Te$_4$, Nano Lett. **23**, 3781 (2023).

[16] Y. Feng, Y. Dai, B. Huang, L. Kou, and Y. Ma, Layer Hall effect in multiferroic two-dimensional materials, Nano Lett. **23**, 5367 (2023).

[17] R. Peng, T. Zhang, Z. He, Q. Wu, Y. Dai, B. Huang, and Y. Ma, Intrinsic layer-polarized anomalous Hall effect in bilayer MnBi$_2$Te$_4$, Phys. Rev. B **107**, 085411 (2023).

[18] K. Liu, X. Ma, S. Xu, Y. Li, and M. Zhao, Tunable sliding ferroelectricity and magnetoelectric coupling in two-dimensional multiferroic MnSe materials, npj Comput. Mater. **9**, 16 (2023).

[19] T. Zhong, L. Cheng, Y. Ren, and M. Wu, Theoretical studies of sliding ferroelectricity, magnetoelectric couplings, and piezo-multiferroicity in two-dimensional magnetic materials, Chem. Phys. Lett. **818**, 140430 (2023).

[20] X. Kong, H. Yoon, M. J. Han, and L. Liang, Switching interlayer magnetic order in bilayer CrI$_3$ by stacking reversal, Nanoscale **13**, 16172 (2021).

[21] B. Huang, G. Clark, E. Navarro-Moratalla, D. R. Klein, R. Cheng, K. L. Seyler, D. Zhong, E. Schmidgall, M. A. McGuire, D. H. Cobden, W. Yao, D. Xiao, P. Jarillo-Herrero, and X. Xu, Layer-dependent ferromagnetism in a van der Waals crystal down to the monolayer limit, Nature (London) **546**, 270 (2017).

[22] M. Fiebig, T. Lottermoser, D. Fröhlich, A. Goltsev, and R. Pisarev, Observation of coupled magnetic and electric domains, Nature (London) **419**, 818 (2002).

[23] Z. Ni, A. V. Haglund, H. Wang, B. Xu, C. Bernhard, D. G. Mandrus, X. Qian, E. J. Mele, C. L. Kane, and L. Wu, Imaging the Néel vector switching in the monolayer antiferromagnet MnPSe$_3$ with strain-controlled Ising order, Nat. Nanotechnol. **16**, 782 (2021).

[24] Z. Sun, Y. Yi, T. Song, G. Clark, B. Huang, Y. Shan, S. Wu, D. Huang, C. Gao, Z. Chen, M. McGuire, T. Cao, D. Xiao, W.-T. Liu, W. Yao, X. Xu, and S. Wu, Giant nonreciprocal second-harmonic generation from antiferromagnetic bilayer CrI$_3$, Nature (London) **572**, 497 (2019).

[25] S. A. Denev, T. T. A. Lummen, E. Barnes, A. Kumar, V. Gopalan, and D. J. Green, Probing ferroelectrics using optical second harmonic generation, J. Am. Ceram. Soc. **94**, 2699 (2011).

[26] O. A. Aktsipetrov, T. V. Misuryaev, T. V. Murzina, L. M. Blinov, V. M. Fridkin, and S. P. Palto, Optical second-harmonic-generation probe of two-dimensional ferroelectricity, Opt. Lett. **25**, 411 (2000).

[27] R.-C. Xiao, D.-F. Shao, W. Gan, H.-W. Wang, H. Han, Z. G. Sheng, C. Zhang, H. Jiang, and H. Li, Classification of second harmonic generation effect in magnetically ordered materials, npj Quantum Mater. **8**, 62 (2023).

[28] H. L. Zhuang, P. R. C. Kent, and R. G. Hennig, Strong anisotropy and magnetostriction in the two-dimensional Stoner ferromagnet Fe$_3$GeTe$_2$, Phys. Rev. B **93**, 134407 (2016).

[29] L. Webster and J.-A. Yan, Strain-tunable magnetic anisotropy in monolayer CrCl$_3$, CrBr$_3$, and CrI$_3$, Phys. Rev. B **98**, 144411 (2018).

[30] C. Gong, L. Li, Z. Li, H. Ji, A. Stern, Y. Xia, T. Cao, W. Bao, C. Wang, Y. Wang, Z. Q. Qiu, R. J. Cava, S. G. Louie, J. Xia, and X. Zhang, Discovery of intrinsic ferromagnetism in two-dimensional van der Waals crystals, Nature (London) **546**, 265 (2017).

[31] S. V. Gerus, A. A. Sokolovskii, A. Y. Mityagin, B. V. Khlopov, and A. S. Kuz'minykh, Stability of magnetooptical disks under the action of external magnetic fields, J. Commun. Technol. Electron. **55**, 1304 (2010).

[32] S. Kawasaki, K. Ishizuka, S. K. Shinichi Katsuda, and M. S. Mitoshi Sohmuta, Magneto-optical disk for magnetic field modulation recording method with multi-pulsed laser irradiation, Jpn. J. Appl. Phys. **32**, 3163 (1993).

[33] J. F. Dillon, Magnetooptics and its uses, J. Magn. Magn. Mater. **31-34**, 1 (1983).

[34] D. Xiang, T. Liu, J. Xu, J. Y. Tan, Z. Hu, B. Lei, Y. Zheng, J. Wu, A. H. C. Neto, L. Liu, and W. Chen, Two-dimensional multibit

optoelectronic memory with broadband spectrum distinction, Nat. Commun. **9**, 2966 (2018).

[35] R. R. Birss, Macroscopic symmetry in space-time, Rep. Prog. Phys. **26**, 307 (1963).

[36] G. Kresse and J. Furthmüller, Efficient iterative schemes for *ab initio* total-energy calculations using a plane-wave basis set, Phys. Rev. B **54**, 11169 (1996).

[37] G. Kresse and D. Joubert, From ultrasoft pseudopotentials to the projector augmented-wave method, Phys. Rev. B **59**, 1758 (1999).

[38] A. A. Mostofi, J. R. Yates, Y.-S. Lee, I. Souza, D. Vanderbilt, and N. Marzari, wannier90: A tool for obtaining maximally-localised Wannier functions, Comput. Phys. Commun. **178**, 685 (2008).

[39] A. A. Mostofi, J. R. Yates, G. Pizzi, Y.-S. Lee, I. Souza, D. Vanderbilt, and N. Marzari, An updated version of wannier90: A tool for obtaining maximally-localised Wannier functions, Comput. Phys. Commun. **185**, 2309 (2014).

[40] See Supplemental Material at http://link.aps.org/supplemental/10.1103/PhysRevB.110.125413 for band structure, net magnetic moments, and work function of the bilayer VSe_2 and $MnBi_2Te_4$, the isomorphic group method, the symmetry-adapted anomalous photoconductivity, the calculation method for SHG and Kerr effects, SHG coefficients of the monolayer VSe_2, and oblique incident SHG characteristics for interlayer sliding multiferroic and conventional multiferroic materials, which include Refs. [12,17,27,35,47–60].

[41] F. Nastos, B. Olejnik, K. Schwarz, and J. E. Sipe, Scissors implementation within length-gauge formulations of the frequency-dependent nonlinear optical response of semiconductors, Phys. Rev. B **72**, 045223 (2005).

[42] Y. Yao, L. Kleinman, A. H. MacDonald, J. Sinova, T. Jungwirth, D. S. Wang, E. Wang, and Q. Niu, First principles calculation of anomalous Hall conductivity in ferromagnetic bcc Fe, Phys. Rev. Lett. **92**, 037204 (2004).

[43] G. Pizzi, V. Vitale, R. Arita, S. Blügel, F. Freimuth, G. Géranton, M. Gibertini, D. Gresch, C. Johnson, T. Koretsune, J. Ibañez-Azpiroz, H. Lee, J.-M. Lihm, D. Marchand, A. Marrazzo, Y. Mokrousov, J. I. Mustafa, Y. Nohara, Y. Nomura, L. Paulatto *et al.*, Wannier90 as a community code: New features and applications, J. Phys.: Condens. Matter **32**, 165902 (2020).

[44] C. Wang, X. Liu, L. Kang, B.-L. Gu, Y. Xu, and W. Duan, First-principles calculation of nonlinear optical responses by Wannier interpolation, Phys. Rev. B **96**, 115147 (2017).

[45] J. Ibañez-Azpiroz, S. S. Tsirkin, and I. Souza, *Ab initio* calculation of the shift photocurrent by Wannier interpolation, Phys. Rev. B **97**, 245143 (2018).

[46] H. T. Stokes and D. M. Hatch, FINDSYM: Program for identifying the space-group symmetry of a crystal, J. Appl. Crystallogr. **38**, 237 (2005).

[47] S. V. Gallego, E. S. Tasci, G. de la Flor, J. M. Perez-Mato, and M. I. Aroyo, Magnetic symmetry in the Bilbao Crystallographic Server: A computer program to provide systematic absences

[48] S. V. Gallego, J. Etxebarria, L. Elcoro, E. S. Tasci, and J. M. Perez-Mato, Automatic calculation of symmetry-adapted tensors in magnetic and non-magnetic materials: A new tool of the Bilbao Crystallographic Server, Acta Crystallogr. A: Found. Adv. **75**, 438 (2019).

[49] A. Gao, Y.-F. Liu, C. Hu, J.-X. Qiu, C. Tzschaschel, B. Ghosh, S.-C. Ho, D. Bérubé, R. Chen, H. Sun, Z. Zhang, X.-Y. Zhang, Y.-X. Wang, N. Wang, Z. Huang, C. Felser, A. Agarwal, T. Ding, H.-J. Tien, A. Akey *et al.*, Layer Hall effect in a 2D topological axion antiferromagnet, Nature (London) **595**, 521 (2021).

[50] R. Chen, H.-P. Sun, M. Gu, C.-B. Hua, Q. Liu, H.-Z. Lu, and X. C. Xie, Layer Hall effect induced by hidden Berry curvature in antiferromagnetic insulators, Natl. Sci. Rev. **11**, nwac140 (2022).

[51] R. Fei, W. Song, and L. Yang, Giant photogalvanic effect and second-harmonic generation in magnetic axion insulators, Phys. Rev. B **102**, 035440 (2020).

[52] H. Chen, M. Ye, N. Zou, B.-L. Gu, Y. Xu, and W. Duan, Basic formulation and first-principles implementation of non-linear magneto-optical effects, Phys. Rev. B **105**, 075123 (2022).

[53] S. Kovachev and J. M. Wesselinowa, Impact of the spin–phonon interaction on the phonon properties of multiferroic hexagonal $RMnO_3$ thin films, J. Phys.: Condens. Matter **22**, 255901 (2010).

[54] J. Fontcuberta, Multiferroic $RMnO_3$ thin films, C. R. Phys. **16**, 204 (2015).

[55] D. Zhang, A. Li, X. Chen, W. Zhou, and F. Ouyang, Tuning valley splitting and magnetic anisotropy of multiferroic $CuMP_2X_6$ (M = Cr,V; X = S,Se) monolayer, Phys. Rev. B **105**, 085408 (2022).

[56] J. S. Qi, H. Wang, X. F. Chen, and X. F. Qian, Two-dimensional multiferroic semiconductors with coexisting ferroelectricity and ferromagnetism, Appl. Phys. Lett. **113**, 043102 (2018).

[57] T. Varga, T. C. Droubay, L. Kovarik, M. I. Nandasiri, V. Shutthanandan, D. H. Hu, B. Kim, S. Jeon, S. Hong, Y. L. Li, and S. A. Chambers, Coupled lattice polarization and ferromagnetism in Multiferroic $NiTiO_3$ thin films, ACS Appl. Mater. Interfaces **9**, 21879 (2017).

[58] T. Varga, T. C. Droubay, M. E. Bowden, P. Nachimuthu, V. Shutthanandan, T. B. Bolin, W. A. Shelton, and S. A. Chambers, Epitaxial growth of $NiTiO_3$ with a distorted ilmenite structure, Thin Solid Films **520**, 5534 (2012).

[59] T. Varga, T. C. Droubay, L. Kovarik, D. Hu, and S. A. Chambers, Controlling the structure and ferroic properties of strained epitaxial $NiTiO_3$ thin films on sapphire by post-deposition annealing, Thin Solid Films **662**, 47 (2018).

[60] W.-Y. Tong, S.-J. Gong, X. Wan, and C.-G. Duan, Concepts of ferrovalley material and anomalous valley Hall effect, Nat. Commun. **7**, 13612 (2016).